

# Differential Astrometry of Sub-arcsecond Scale Binaries at the Palomar Testbed Interferometer

B. F. Lane, M. W. Muterspaugh

*Center for Space Research  
MIT Department of Physics  
70 Vassar Street, Cambridge, MA 02139*

blane@mit.edu

matthew1@mit.edu

## ABSTRACT

We have used the Palomar Testbed Interferometer to perform very high precision differential astrometry on the 0.25 arcsecond separation binary star HD 171779. In 70 minutes of observation we achieve a measurement uncertainty of  $\approx 9$  micro-arcseconds in one axis, consistent with theoretical expectations. Night-to-night repeatability over four nights is at the level of 16 micro-arcseconds. This method of very-narrow-angle astrometry may be extremely useful for searching for planets with masses as small as  $0.5 M_{Jup}$  around a previously neglected class of stars – so-called “speckle binaries.” It will also provide measurements of stellar parameters such as masses and distances, useful for constraining stellar models at the  $10^{-3}$  level.

*Subject headings:* techniques:interferometric–techniques:astrometry

## 1. Introduction

Long-baseline optical interferometry promises high precision astrometry using modest ground-based instruments. In particular the Mark III Stellar Interferometer (Shao et al. 1988) and Navy Prototype Optical Interferometer (NPOI, Armstrong et al. 1998) have achieved global astrometric precision at the 10 mas ( $1 \text{ mas} = 10^{-3}$  arcseconds) level (Hummel et al. 1994), while the Palomar Testbed Interferometer (PTI, Colavita et al. 1999) has demonstrated an astrometric precision of  $100 \mu\text{as}$  ( $1 \mu\text{as} = 10^{-6}$  arcseconds) between moderately close (30 arcsecond) pairs of bright stars (Shao & Colavita 1992; Colavita 1994; Lane et al. 2000). While interferometric and astrometric methods have proven very useful

in studying binary stars, and have long been argued to be well-suited to studying extra-solar planets (Colavita & Shao 1994; Eisner & Kulkarni 2001), to date results using these techniques have been limited (Benedict et al. 2002b).

There are several reasons why it is desirable to develop viable astrometric planet-detection methods. Most importantly, the parameter space explored by astrometry is complementary to that of radial velocity (astrometry is more sensitive to larger separations). Second, unlike current radial velocity detections, astrometric techniques can be used to determine the orbital inclination of a planet. Finally, astrometry is particularly well-suited to studying binary stellar systems; such systems challenge other planet-finding techniques. For example, radial velocimetry can suffer from systematic velocity errors caused by spectral contamination from the light of the second star (Vogt et al. 2000). Similar problems are faced by coronagraphic techniques, where the light from the second star is not usually blocked by the occulting mask.

In this paper we describe recent efforts to obtain very high precision narrow-angle astrometry using PTI to observe binary stars with separations less than one arcsecond, i.e. systems that are typically observed using speckle interferometry (Saha 2002) or adaptive optics. Such small separations allow us to achieve astrometric precision on the order of 10  $\mu$ as, which for a typical binary system in our target sample (binary separation of 20 AU), should allow us to detect planets with masses down to 0.5 Jupiter masses in orbits in the 2 AU range. This approach has been suggested (Traub, Carleton & Porro 1996) and tried (Dyck, Benson & Schloerb 1995; Bagnuolo et al. 2003) before, though with limited precision. However, this work is unique in that it makes use of a phase-tracking interferometer; the use of phase-referencing (Lane & Colavita 2003) removes much of the effect of atmospheric turbulence, improving the astrometric precision by a factor of order 100.

The Palomar Testbed Interferometer (PTI) is located on Palomar Mountain near San Diego, CA (Colavita et al. 1999). It was developed by the Jet Propulsion Laboratory, California Institute of Technology for NASA, as a testbed for interferometric techniques applicable to the Keck Interferometer and other missions such as the Space Interferometry Mission, SIM. It operates in the J ( $1.2\mu$ m), H ( $1.6\mu$ m) and K ( $2.2\mu$ m) bands, and combines starlight from two out of three available 40-cm apertures. The apertures form a triangle with 86 and 110 meter baselines.

The paper is organized as follows: in Section 2 we describe the experiment and derive expected performance levels. In Section 3 we describe initial observations as well as the extensive data analysis processing required to achieve the desired astrometric precision. In Section 4 we discuss our preliminary results, and in Section 5 we discuss the prospects of a larger search.

## 2. Interferometric Astrometry

In an optical interferometer light is collected at two or more apertures and brought to a central location where the beams are combined and a fringe pattern produced. For a broadband source of wavelength  $\lambda$  the fringe pattern is limited in extent and appears only when the optical paths through the arms of the interferometer are equalized to within a coherence length ( $\Lambda = \lambda^2/\Delta\lambda$ ). For a two-aperture interferometer, neglecting dispersion, the intensity measured at one of the combined beams is given by

$$I(\delta) = I_0 \left( 1 + V \frac{\sin(\pi\delta/\Lambda)}{\pi\delta/\Lambda} \sin(2\pi\delta/\lambda) \right) \quad (1)$$

where  $V$  is the fringe contrast or “visibility”, which can be related to the morphology of the source, and  $\Delta\lambda$  is the optical bandwidth of the interferometer assuming a flat optical bandpass (for PTI  $\Delta\lambda = 0.4\mu\text{m}$ ). The differential (between arms of the interferometer) optical path  $\delta$  is found from geometric considerations to be

$$\delta = \vec{B} \cdot \vec{s} - d \quad (2)$$

$\vec{B}$  is the baseline – the vector connecting the two apertures.  $\vec{s}$  is the unit vector in the source direction, and  $d$  is any differential optical path introduced by the instrument. For a 100-m baseline interferometer an astrometric precision of 10  $\mu\text{as}$  corresponds to knowing  $d$  to 5 nm, a difficult but not impossible proposition.

The dominant source of measurement error is atmospheric turbulence above the interferometer, which adds varying amounts of optical path and hence makes the fringes appear to move about rapidly (Roddier 1981). This atmospheric turbulence, which changes over distances of tens of centimeters and millisecond time-scales, forces one to use very short exposures to maintain fringe contrast, and hence limits the sensitivity of the instrument. It also severely limits the astrometric accuracy of a simple interferometer, at least over large sky angles. However, this atmospheric turbulence is correlated over small angles, and hence it is still possible to obtain high precision “narrow-angle” astrometry.

### 2.1. Narrow-Angle Astrometry

Dual-star interferometric narrow-angle astrometry (Shao & Colavita 1992; Colavita 1994) promises astrometric performance at the 10-100  $\mu\text{as}$  level for pairs of stars separated by 10-60 arcseconds, and has been demonstrated at PTI. Achieving such performance requires simultaneous measurements of the fringe positions of both stars via the use of a “dual-star” optical beam-train.

For more closely spaced stars, it is possible to operate in a simpler mode. We have recently used PTI to observe pairs of stars separated by no more than one arcsecond. In this mode, the small separation of the binary results in both binary components being in the field of view of a single interferometric beam combiner. The fringe positions are measured by modulating the instrumental delay with an amplitude large enough to record both fringe packets. This eliminates the need for a complex internal metrology system to measure the entire optical path of the interferometer, and dramatically reduces the effect of systematic error sources such as uncertainty in the baseline vector (error sources which scale with the binary separation).

However, since the fringe position measurement of the two stars is no longer truly simultaneous it is possible for the atmosphere to introduce pathlength changes (and hence positional error) in the time between measurements of the separate fringes. To reduce this effect we split off a fraction of the incoming starlight and direct it to a second beam-combiner. This beam-combiner is used in a “fringe-tracking” mode (Shao & Staelin 1980; Colavita et al. 1999) where it rapidly (10 ms) measures the phase of one of the starlight fringes, and adjusts the internal delay to keep that phase constant. This technique – known as phase referencing – has the effect of stabilizing the fringe measured by the astrometric beam-combiner. In addition, the residual phase error measured by the fringe tracker is a high time-resolution trace of the phase error introduced by the atmosphere and not fully corrected by the fringe tracker; it can be applied to the measured fringe position in post-processing.

## 2.2. Expected Performance

In making an astrometric measurement we modulate the optical delay applied internally in a triangle-wave pattern around the stabilized fringe position, while measuring the intensity of the combined starlight beams. Typically we obtain one such “scan” every 1-3 seconds, consisting of up to 3000 intensity samples. The range of the delay sweep is set to include both fringe packets; typically this requires a scan amplitude on the order of  $100\ \mu\text{m}$ . We then fit a double fringe packet based on Eqn. 1 to the data, and solve for the differential optical path between fringe packets.

In calculating the expected astrometric performance we take into account three major sources of error: errors caused by fringe motion during the sweep between fringes (loss of coherence with time), errors caused by differential atmospheric turbulence (loss of coherence with sky angle, i.e. anisoplanatism), and measurement noise in the fringe position. We quantify each in turn below, and the expected measurement precision is the root-sum-squared of the terms (Figure 2).

### 2.2.1. Loss of Temporal Coherence

The power spectral density of the fringe phase of a source observed through the atmosphere has a power-law dependence on frequency (Figure 1); at high frequencies typically

$$A(f) \propto f^{-\alpha} \quad (3)$$

where  $\alpha$  is usually in the range 2.5–2.7. The effect of phase-referencing is to high-pass filter this atmospheric phase noise. In our case, the servo is an integrating servo with finite processing delays and integration times, with the residual phase error “fed forward” to the second beam combiner (Lane & Colavita 2003). The response of this system to an input atmospheric noise can be written in terms of frequency (see Appendix A in Lane 2003) as

$$H(f) = \frac{1 - 2\text{sinc}(\pi f T_s) \cos(2\pi f T_d) + \text{sinc}^2(\pi f T_s)}{1 - 2\frac{f_c}{f} \text{sinc}(\pi f T_s) \sin(2\pi f T_d) + \left(\frac{f_c}{f}\right)^2 \text{sinc}^2(\pi f T_s)} \quad (4)$$

where  $\text{sinc}(x) = \sin(x)/x$ ,  $f_c$  is the closed-loop bandwidth of the fringe-tracker servo (for this experiment  $f_c = 10$  Hz),  $T_s$  is the integration time of the phase sample (6.75 ms), and  $T_d$  is the delay between measurement and correction (done in post-processing, effectively 5 ms). The phase noise superimposed on the double fringe measured by the astrometric beam combiner has a spectrum given by  $A(f)H(f)$ .

The sampling of the double fringe packet takes a finite amount of time, first sampling one fringe, then the other. In the time domain the sampling function can be represented as a “top-hat” function convolved with a pair of delta functions (one positive, one negative). The width of the top-hat is equal to the time taken to sweep through a single fringe, while the separation between the delta functions is equal to the time to sweep between fringes. In the frequency domain this sampling function becomes

$$S(f) = \sin^2(2\pi f \tau_p) \text{sinc}^2(\pi f \tau_*) \quad (5)$$

where  $\tau_p$  is the time taken to move the delay between stars,  $\Delta d/v_s$ , and  $\tau_*$  is the time to sweep through a single stellar fringe,  $\Lambda/v_s$ .  $v_s$  is the delay sweep rate.

The resulting error in the astrometric measurement, given in radians by  $\sigma_{tc}$ , can be found from

$$\sigma_{tc}^2 = \left(\frac{\lambda}{2\pi B}\right)^2 \frac{1}{N} \int_0^\infty A(f)H(f)S(f)df \quad (6)$$

where  $N$  is the number of measurements. It is worth noting that if phase-referencing is not used to stabilize the fringe, i.e.  $H(f) = 1$ , the atmospheric noise contribution increases by a factor of  $\approx 10^2$ – $10^3$ .

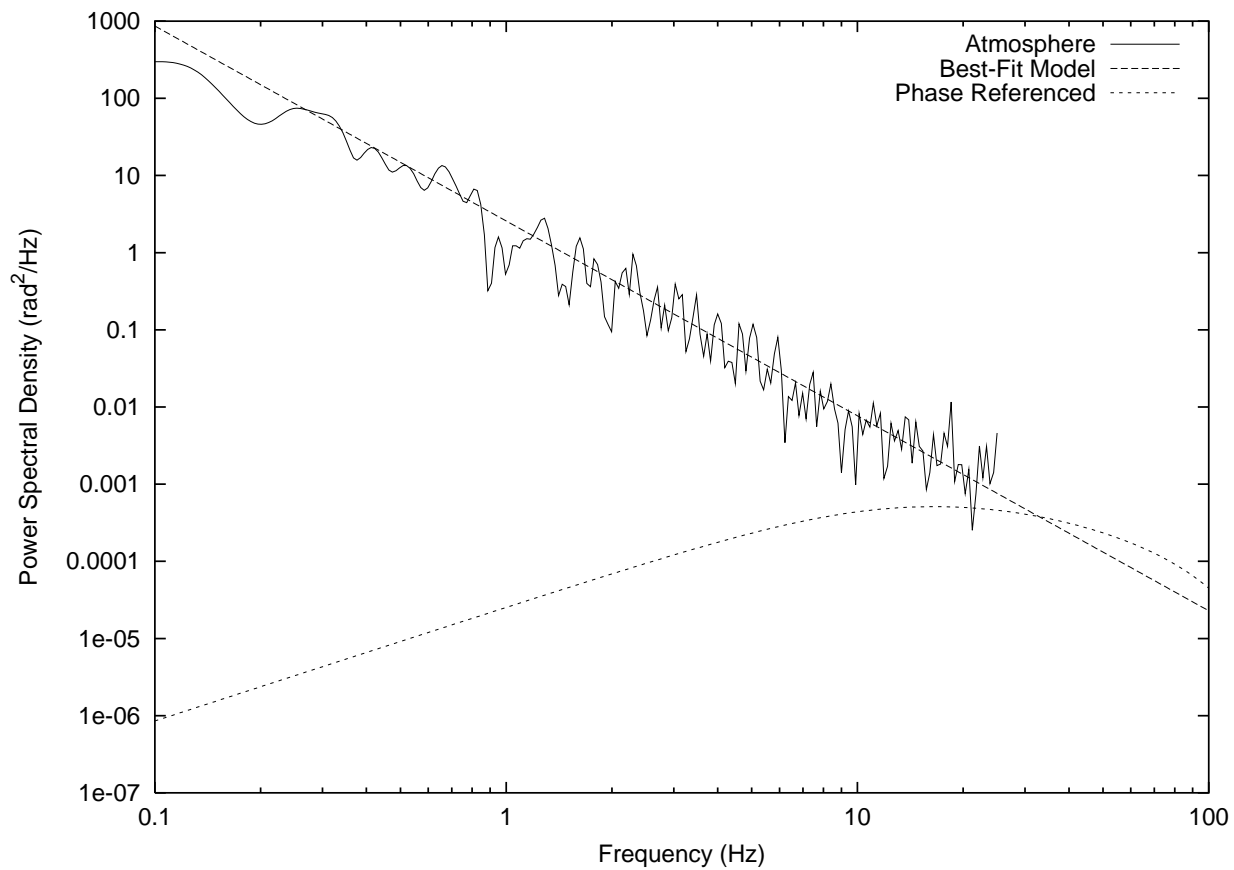


Fig. 1.— Power spectral density of the fringe phase as measured by PTI (Lane & Colavita 2003). The phase PSD is best fit by a power law  $A(f) \propto f^{-2.5}$ . Also shown is the effective PSD of the phase noise after phase referencing has stabilized the fringe.

### 2.2.2. Anisoplanatism

The performance of a simultaneous narrow-angle astrometric measurement has been thoroughly analyzed in Shao & Colavita (1992). Here we restate the primary result for the case of typical seeing at a site such as Palomar Mountain, where the astrometric error in arcseconds due to anisoplanatism ( $\sigma_a$ ) is given by

$$\sigma_a = 540B^{-2/3}\theta t^{1/2} \quad (7)$$

where  $B$  is the baseline,  $\theta$  is the angular separation of the stars, and  $t$  the integration time in seconds. This assumes a standard (Lindgren 1980) atmospheric turbulence profile; it is likely that particularly good sites will have somewhat (factor of two) better performance.

### 2.2.3. Photon Noise

The astrometric error due to photon-noise ( $\sigma_p$ ) is given in radians as

$$\sigma_p = \frac{\lambda}{2\pi B} \frac{1}{\sqrt{N}} \frac{1}{\text{SNR}} \quad (8)$$

where  $N$  is the number of fringe scans, and SNR is the signal-to-noise ratio of an individual fringe.

## 3. Observations & Data Processing

We used the Palomar Testbed Interferometer to observe the binary star HD 171779 (HR 6983, K0III+G9III,  $m_K = 2.78$ ,  $m_V = 5.37$ ) on the nights of 11-14 August 2003. Conditions were calm with good seeing although with high-altitude clouds limiting observations, particularly after the first night. Based on a visual orbit obtained from speckle interferometry (Hartkopf et al. 2001), the predicted separation was 0.248 arcsec at a position-angle of 120.9 degrees. The orbit quality was listed as 3 (on a scale of 1–5), indicating a “reliable” orbit, though no uncertainties are given. The published  $\Delta V = 0.21$  (Worley, Mason & Wycoff 2001), and the orbital period is 191.49 years.

We used the longest available baseline (110 m). The observations were done in the K band ( $2.2\mu\text{m}$ ), with  $\approx 70\%$  of the K-band light being used for fringe tracking, and the remaining light going to the astrometric measurement. The fringe tracker operated in the standard configuration (Colavita et al. 1999), with a sample time of 10 ms and a closed-loop servo bandwidth of  $\approx 10$  Hz. The delay modulation used for the astrometric measurement

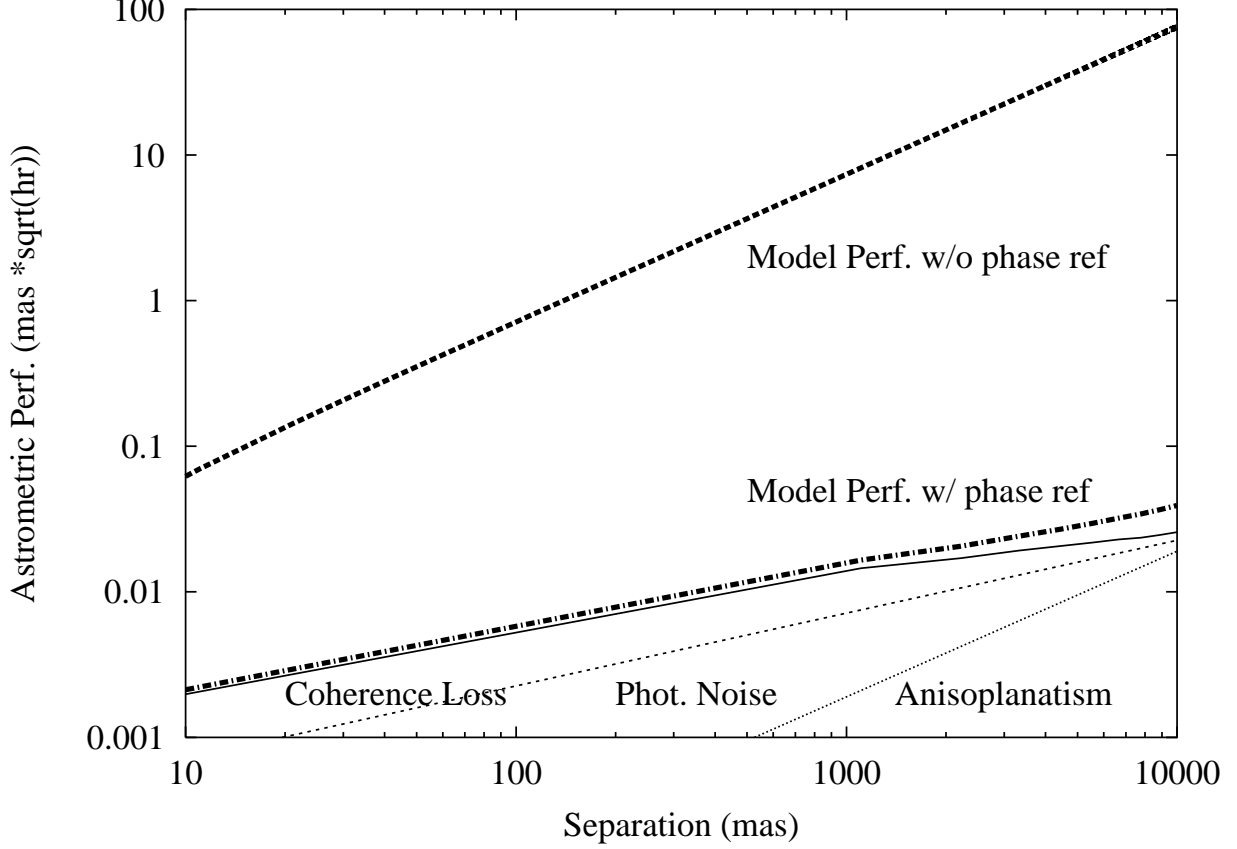


Fig. 2.— The expected narrow-angle astrometric performance in mas for the phase-referenced fringe-scanning approach, for a fixed delay sweep rate, and an interferometric baseline of 110 m. The three error sources are described in Section 2.2. Also shown is the magnitude of the temporal loss of coherence effect in the absence of phase referencing, illustrating why stabilizing the fringe via phase referencing is necessary.



typically had an amplitude of  $150\ \mu\text{m}$  and period of 3 seconds. The modulation was done using a PZT-actuated mirror, the position of which was measured using a laser metrology system.

The intensity vs. delay position measurements produced by the interferometer were processed into astrometric measurements as follows: (1) Detector calibrations (gain, bias and background) were applied to the intensity measurements. (2) The residual phase errors from the primary fringe tracker were converted to delay and applied to the data. Note that while the intensity measurements were spaced regularly in time, and the delay scanned linearly in time, the variable amount of delay correction applied from the fringe tracker resulted in the intensity measurements being unevenly spaced in delay. This somewhat complicated the downstream processing, in that FFT-based algorithms could not be used. (3) The data were broken up into “scans” either when the delay sweep changed direction or when the fringe tracker lost lock. (4) For each scan, a power spectrum was calculated using a Lomb-Scargle (Scargle 1982; Press et al. 1992) algorithm. This spectrum provided an SNR estimate based on the ratio of the power in and out of the instrument bandpass. Only the scans with an SNR greater than unity were kept. (5) The intensity measurements were optionally bandpass-filtered to remove the effects of atmospheric turbulence changing the amount of light being coupled into the detector. We note however that the final results of the fit (see below) did not depend on whether or not the filter was applied; the results differed by  $\ll 1\sigma$  (the results shown were based on unfiltered data). See Figure 3 for an example of filtered fringes. (6) The differential delay of each scan was found by evaluating the least-squares goodness-of-fit ( $\chi^2$ ) parameter for a fit of a double fringe packet to each scan, for the range of plausible delay separations and mean delay values, and selecting the separation corresponding to the  $\chi^2$ -minimum. See the discussion below for how plausible ranges were determined. (7) Given a set of delay separations as a function of time, a simple astrometric model was fit to the data. The free parameters were separation and position angle, or equivalently, differential right ascension and declination (Figure 4).

In order to characterize any systematic dependence on assumptions made in the data reduction, such as the shape of the fringe envelope, the effect of dispersion, the effect of filtering and the level of the fringe SNR-cutoff, we exhaustively varied these parameters and re-fit the data each time. In all cases the effect was small compared to the claimed uncertainties. This suggests that our results are robust against systematic errors in the data processing algorithm; many potential systematic error sources are eliminated due to the differential nature of the measurement.

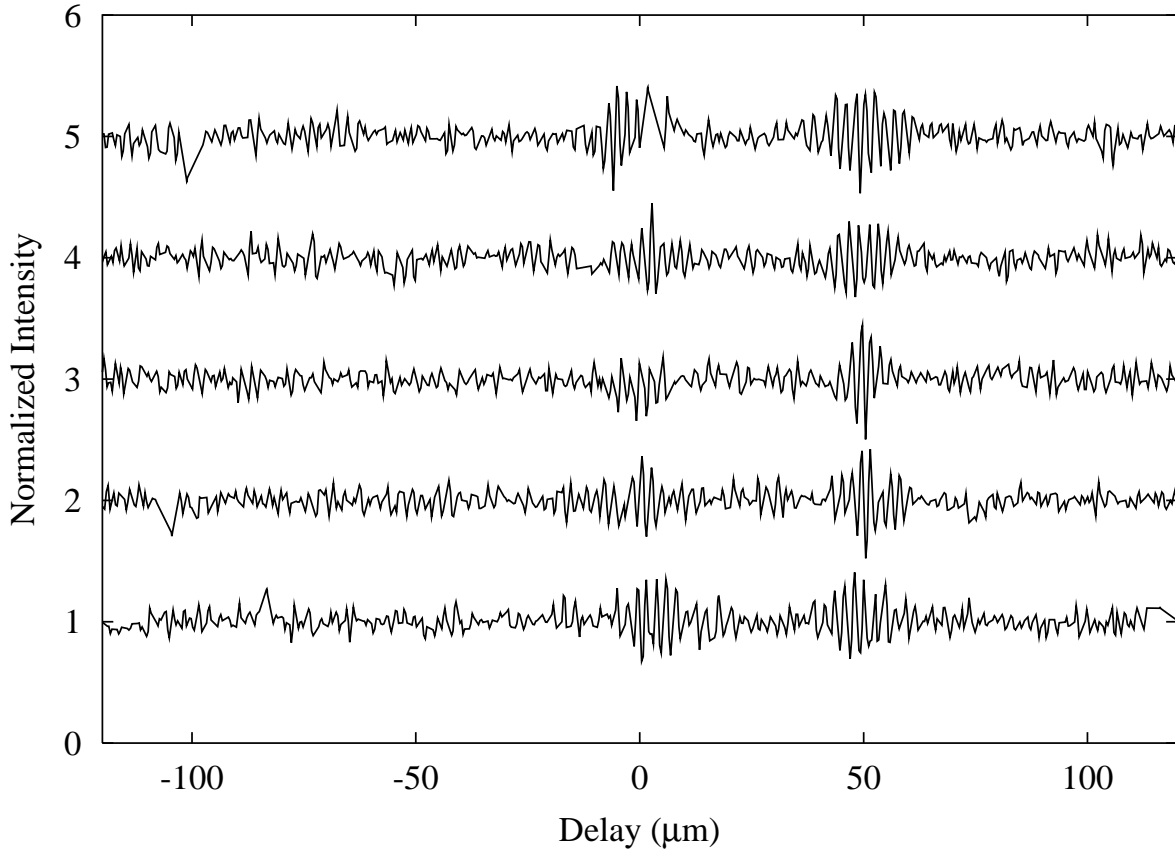


Fig. 3.— A plot showing five consecutive filtered fringe scans of HD 171779. Each scan corresponds to  $\sim 1.5$  seconds of data. The scans have been normalized, and offset for clarity.

### 3.1. Resolving Fringe Ambiguity

The oscillatory nature of the fringe means that there will be many local minima in the  $\chi^2$  surface, separated from the global minimum (at the center of the fringe packet) by integer multiples of the wavelength  $\lambda$ . In the presence of noise it is not always obvious which is the global minimum. In previous work (Dyck, Benson & Schloerb 1995) this ambiguity was avoided by forming an “envelope” of the fringe packets, then fitting these envelopes. However, this effectively removed the high-resolution phase information, which is what provides the high precision astrometry.

We find that it is possible to co-add the  $\chi^2(\Delta d)$  functions from many scans. This increases the signal-to-noise ratio and so reduces the likelihood of picking the “wrong” fringe. In order to perform the co-adding, the two-dimensional (separation and mean delay)  $\chi^2$  surface was projected into a one-dimensional space of delay separation by selecting the best (lowest  $\chi^2$ ) mean delay position for each possible delay separation. The minimum of this co-added  $\chi^2$  function was used to determine the fringe separation to within  $\lambda$ ; the range of plausible separations (used in step 6 above) was limited to  $\pm\lambda/2$  around this value.

The number of scans that could be co-added in this manner depended on the rate of change of delay separation, with too long of an integration time “smearing” the fringes. We found that in the case of our observations, co-adding all the  $\chi^2$  functions from a 75-second period gave adequate SNR to reliably (85–95% of the time) determine the central fringe. The remaining 5–15% of scans produced delays that were shifted off the median fringe position by a wavelength. However, rather than artificially adjusting the delays by a multiple of the wavelength, these scans were simply discarded. Note that no *a priori* information was used to constrain the location of the central fringe, and each 75-second group was treated independently.

We also point out that it should be possible to co-add  $\chi^2$  functions not as a function of separation but as a function of differential right ascension and declination; such an approach should allow one to use the co-adding approach with very long integration times (e.g. for all the scans of a given star in a night). We are currently developing such an approach.

## 4. Results

We show the results of an astrometric fit to 45 minutes of data (taken over the course of 70 minutes of observation) in Figures 4 and 6. With 1769 scans used, we find the residual delay errors to be well modeled by a Gaussian distribution with a full-width at half-maximum of  $0.160 \mu\text{m}$ . In order to characterize the residuals, and in particular determine if they could

be considered to be independent, we plot the Allan variance of the residuals in Figure 5. The Allan variance (Thompson et al. 2001) at lag  $l$  is given by

$$\sigma_A^2(l) = \frac{1}{2(M' + 1 - 2l)} \sum_{n=0}^{M'-2l} \left( \frac{1}{l} \sum_{m=0}^{l-1} x_{n+m} - x_{n+l+m} \right)^2 \quad (9)$$

where  $M'$  is the total number of data points. As can be seen in the figure, the residuals are white out to lags of more than 500 scans, implying a final astrometric precision of 10  $\mu\text{as}$ . We list the results from 4 nights of observation in Table 1.

The 1-sigma error region (found by plotting the  $\chi^2 = \chi_{min}^2 + \Delta\chi^2$  contour, Press et al. 1992) is highly elliptical with the major axis oriented roughly parallel to the R.A. axis. Such error ellipses are to be expected in single-baseline interferometric data, which has limited sensitivity in the direction perpendicular to the baseline. It should be noted however that for sufficiently long observations, Earth-rotation will provide an orthogonal baseline. The major and minor axes of the uncertainty ellipse are easily found by diagonalizing the covariance matrix: the magnitude of the uncertainty in the direction of the minor axis was 8.3  $\mu\text{as}$  for the 10 August data and 12  $\mu\text{as}$  for the 11 August data; consistent with the delay residuals. The uncertainty in the major axis direction was 144 and 143  $\mu\text{as}$  respectively. Figure 6 shows the four error ellipses superimposed. We fit the measured differential declinations to a linear trend of  $-18 \pm 7 \mu\text{as/day}$ ; the *r.m.s.* of the residuals is 16  $\mu\text{as}$ , and the reduced  $\chi^2 = 1.1$ . The predicted change in differential declination due to orbital motion is approximately  $-11 \mu\text{as/day}$ .

## 5. Discussion

We have achieved an astrometric measurement precision of  $\approx 9 \mu\text{as}$  in 70 minutes of observation on the 0.25 arcsecond separation binary star HD 171779. The measurements were repeated on four nights, yielding answers consistent at the level of 16  $\mu\text{as}$ . These early

Epoch of Observation (MJD)	$\Delta$ R.A. (arcsec)	$\Delta\delta$ (arcsec)	# Scans	<i>rms</i> $\mu\text{m}$
52862.30085	$0.222109 \pm 1.43 \times 10^{-4}$	$-0.119309 \pm 8.39 \times 10^{-6}$	1769	0.160
52863.28229	$0.222233 \pm 1.43 \times 10^{-4}$	$-0.119302 \pm 1.55 \times 10^{-5}$	668	0.162
52864.31096	$0.222134 \pm 1.97 \times 10^{-4}$	$-0.119323 \pm 1.89 \times 10^{-5}$	724	0.163
52865.29921	$0.221981 \pm 1.55 \times 10^{-4}$	$-0.119361 \pm 1.48 \times 10^{-5}$	731	0.200

Table 1: The results from four nights of differential astrometry of the binary HD 171779.

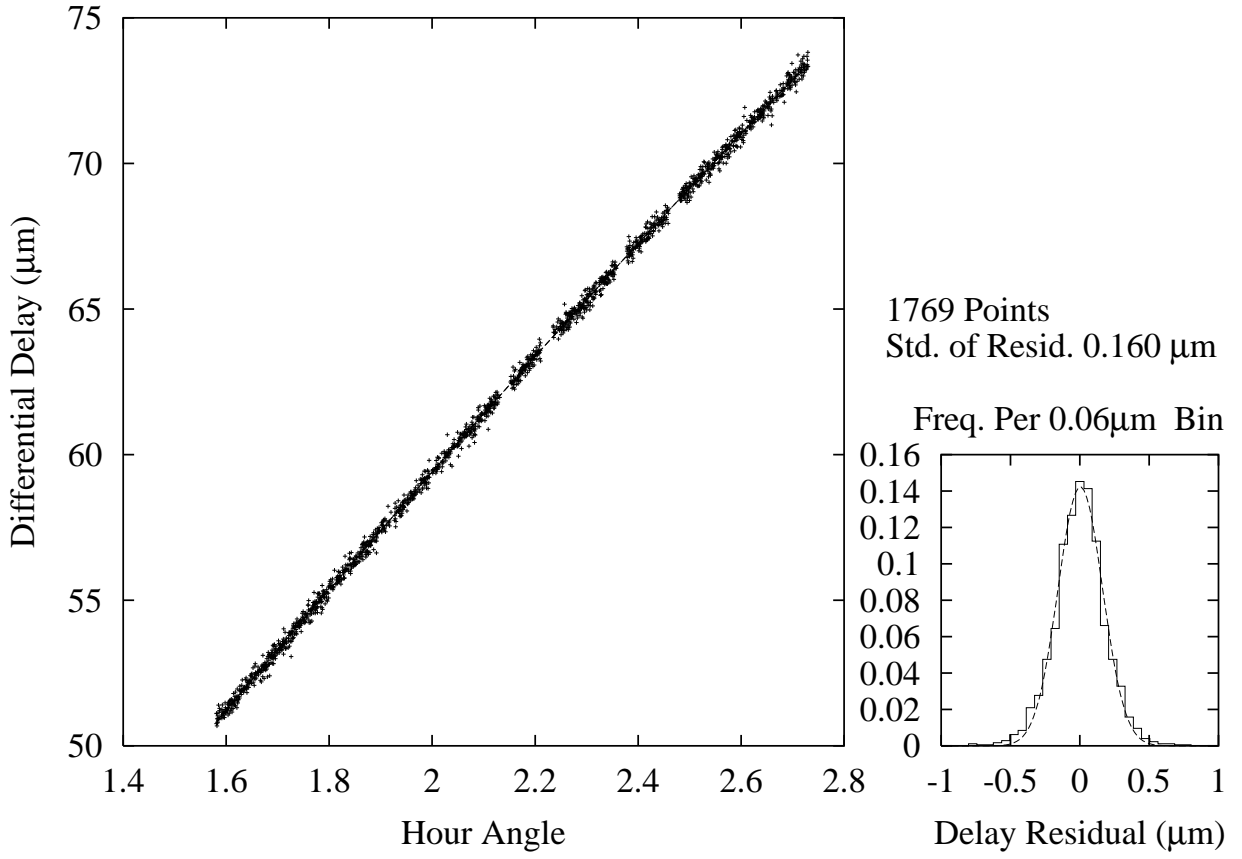


Fig. 4.— A fit of an astrometric separation model to the measured separations as a function of time. Also shown is a histogram of the fit residuals, which are well modeled by a Gaussian distribution.

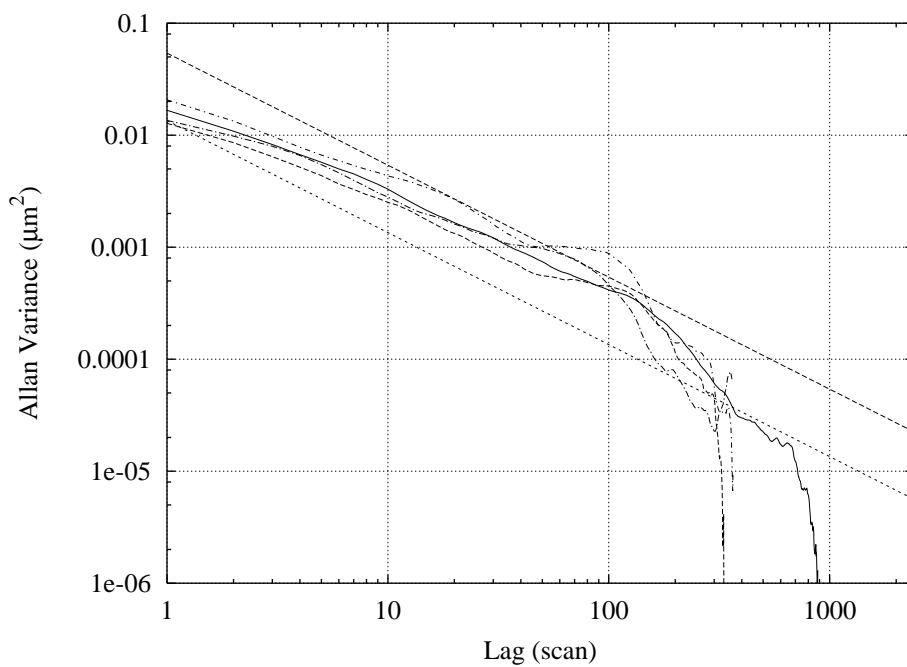


Fig. 5.— Allan variances of the residuals to the astrometric fits, as well as a line showing the expected behavior corresponding to white noise at a level equivalent to a fit precision of  $10 \mu\text{as}$  (upper) and  $5 \mu\text{as}$  (lower) in in 1 hour of integration (1.5 second scans).

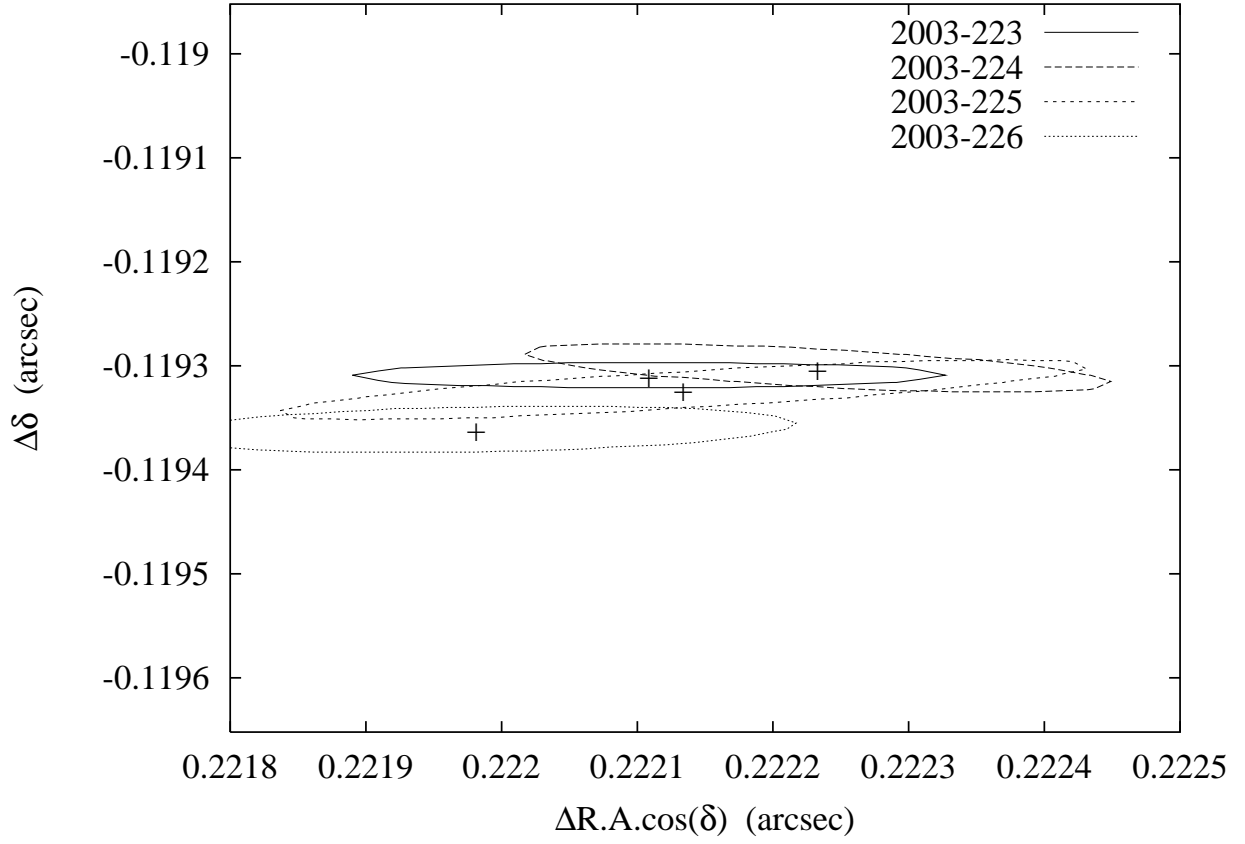


Fig. 6.— A contour plot of the  $\chi^2$  surfaces as a function of the fit parameters, for data from four nights. The 1- $\sigma$  contours and the preferred solutions are marked.

results show the promise of very narrow-angle astrometry for achieving very high precision measurements of stellar binaries with a separations on the order of 0.05–1 arcseconds. This is particularly useful in searching for planets around such binaries, although the resulting high-precision visual orbits for these stars should also be useful in providing stellar masses and distances at the level of  $10^{-3}$ . It should be noted that such high precision mass determinations may require an extended period of observation as these systems can have very long orbital periods. It is also necessary to obtain radial velocity data accurate to 10 m/s or better, which can be challenging.

This newly demonstrated approach to narrow-angle astrometry compares quite favorably with other astrometric methods used to date, such as speckle interferometry (Horsch et al. 2002; Woitas et al. 2003), single-telescope astrometry with (Lane et al. 2001) and without (Pravdo & Shaklan 1996, 2000) adaptive-optics, and space-based astrometry using HST (Benedict et al. 2002a). These have all produced measurement precisions on the order of 0.1-1 mas. The improved performance of the interferometric approach is primarily due to the longer available baseline. However, the combination of phase-referencing and fringe-scanning also compares favorably to other interferometric methods, such as using fringe visibility measurements to find binary star orbits (i.e. a fractional precision of  $10^{-4}$  as compared to  $10^{-2}$ , Boden et al., 2000). In this case the improvement comes from the unbiased nature of the phase estimator.

Recent years have seen a veritable explosion in the number of known extra-solar planets (Schneider 2003), starting with the famous example of 51 Peg (Mayor & Queloz 1995). To date, most of these systems have been found using high-precision radial velocity techniques, although recent photometric transit searches have observed several planets (Charbonneau et al. 2000; Konacki et al. 2003). However, these methods have to a large extent avoided searching close (separation less than a few arcseconds) binary stellar systems, primarily because the techniques used are not well suited to such systems. Therefore it is particularly interesting to note that despite the deliberate avoidance of binaries, of the more than 100 known planets, 14 of them are in wide binary stellar systems. In addition, given the high frequency of binary stellar systems (57% among systems older than 1 Gyr, Duquennoy & Mayor (1991)), it is clear that any comprehensive planetary census must address the question of how frequently planets occur in such systems. This is all the more relevant given that several theoretical investigations have indicated that there exist regions in binary parameter space where planets can form and exist in stable orbits over long periods of time, though this does remain controversial (Whitmire et al. 1998; Boss 1998; Marzari & Scholl 2000; Nelson 2000; Barbieri, Marzari & Scholl 2002).

An instrument such as PTI, capable of 10  $\mu$ as very-narrow-angle astrometry, could be



used to search many of the brightest speckle binary systems for planets. We have compiled a list of approximately 50 suitable systems, with  $m_K < 4.5$ , separations less than 1 arcsecond, and within the field of regard of PTI. The median orbital separation between the binary components in these systems is 19 AU, and hence there should be regions where planets can remain stable for long periods. In particular, adopting the result from Holman & Wiegert (1999) we calculate the largest stable orbit in each system. We find that the median detectable planetary mass in such an orbit is 0.5 Jupiter masses (assuming  $3\sigma$  confidence detections). The corresponding median orbital period is 2.2 years. A limited survey could quickly begin to provide useful constraints on the frequency of planets in binary stellar systems. As a new generation of long-baseline optical interferometers become operational in the next few years, this type of survey could be easily extended to sample sizes of several hundred stars, hence providing strong constraints on planetary formation in the binary environment.

We would like to thank E. Bertschinger, A. Boden, B. F. Burke, M. Colavita, M. Konacki, S. R. Kulkarni & N. Safizadeh for their contributions to this effort. We also particularly acknowledge the extraordinary efforts of K. Rykoski, whose work in operating and maintaining PTI is invaluable and goes far beyond the call of duty. Observations with PTI are made possible through the efforts of the PTI Collaboration, which we acknowledge. Part of the work described in this paper was performed at the Jet Propulsion Laboratory under contract with the National Aeronautics and Space Administration. Interferometer data was obtained at the Palomar Observatory using the NASA Palomar Testbed Interferometer, supported by NASA contracts to the Jet Propulsion Laboratory. This research has made use of the Simbad database, operated at CDS, Strasbourg, France. MWM acknowledges the support of the Michelson Graduate Fellowship program. BFL acknowledges support from a Pappalardo Fellowship in Physics.

## REFERENCES

- Armstrong, J. T., et al., 1998, *ApJ*, 496, 550-571.
- Bagnuolo, W. G. et al., 2003, *Proc. SPIE*, **4838**, 1061.
- Barbieri, M., Marzari, F., & Scholl, H. 2002, *A&A*, **396**, 219
- Benedict, G. Fritz, McArthur, B. E., Fredrick, L. W., Harrison, T. E., Slesnick, C. L., Rhee, J., Patterson, R. J., Skrutskie, M. F., Franz, O. G., Wasserman, L. H., Jefferys, W.

- H., Nelan, E., van Altena, W., Shelus, P. J., Hemenway, P. D., Duncombe, R. L., Story, D., Whipple, A. L., Bradley, A. J., 2002, *AJ*, **124**, 1695-1705.
- Benedict, G. F., McArthur, B. E., Forveille, T., Delfosse, X., Nelan, E., Butler, R. P., Spiesman, W., Marcy, G., Goldman, B., Perrier, C., Jefferys, W. H., and Mayor, M., 2002, *ApJ*, **581**, 115
- Boden, A., Creech-Eakman, M., and Queloz, D., 2000, *ApJ*, 536, 880-890.
- Boss, A. P. 1998, *BAAS*, **30**, 1057
- Charbonneau, D., Brown, T. M., Latham, D. W., Mayor, M., 2000, *ApJ*, **529**, L45-L48
- Colavita, M. M. 1994, *A&A*, 283, 1027
- Colavita, M. M. & Shao, M. 1994, *Ap&SS*, 212, 385
- Colavita, M. M., et al. 1999, *ApJ*, 510, 505.
- Duquennoy, A. & Mayor, M. 1991, , *A&A*, **248**, 485
- Dyck, H. M.; Benson, J. A.; Schloerb, F. P., 1995, *AJ*, **110**, 1433.
- Eisner, J. A. & Kulkarni, S. R. 2001, *ApJ*, 561, 1107
- Hartkopf, W.I., Mason, B.D., Worley, C.E., 2001a, Sixth Catalog of Orbits of Visual Binary Stars. <http://www.ad.usno.navy.mil/wds/orb6/orb6.html>
- Holman, M. J., Wiegert, P. A.. 1999, *AJ*, **117**, 621.
- Horch, E. P., Robinson, S. E., Meyer, R. D., van Altena, W. F., Ninkov, Z., Piterman, A., 2002, *AJ*, **123**, 3442-3459.
- Hummel, C. A., et al., 1994, *AJ*, **108**, 326
- Konacki, M., Torres, G., Jha, S., Sasselov, D. D., 2003, *Nature*, **412**, 507.
- Lane, B. F., et al., 2000, *Proc. SPIE.*, **4006**, 452.
- Lane, B.F., Zapatero Osorio, M. R., Britton, M. C., Martin, E. L., Kulkarni, S. R., 2001, *ApJ* 560, 390–399.
- Lane, B. F., 2003, PhD. Thesis, California Inst. of Technology.
- Lane, B. F., Colavita, M.M., 2003, *AJ*, 125, 1623-1628.

- Lindegren, L. 1980, *A&A*, **89**, 41
- Marzari, F. & Scholl, H. 2000, *ApJ*, **543**, 328
- Mayor, M., Mazeh, T., 1987, *A&A*, **171**, 157-177.
- Mayor, M. & Queloz, D. 1995, *Nature*, **378**, 355
- Nelson, A. F. 2000, *ApJ*, **537**, L65
- Pravdo, S. H. , Shaklan, S. B. 2000, *BAAS*, 197, 62.01
- Pravdo, S. H. & Shaklan, S. B. 1996, *ApJ*, 465, 264
- Press, W.H., Teukolsky, S.A., Vetterling, W.T., Flannery, B.P. 1992, *Numerical Recipes* (New York: Cambridge Univ. Press).
- Roddier, F., in *Progress in Optics*, 1981, ed. E. Wolf (Amsterdam: North-Holland), 281.
- Swapan K. Saha, *Reviews of Modern Physics* 74 (2), 551-600 (2002).
- Scargle, J. D., 1982, *ApJ*, **263**, 835-853.
- Schneider, J., 2003, *The Extrasolar Planets Encyclopaedia*, <http://www.obspm.fr/encycl/encycl.html>
- Shao, M., Staelin, D. H., 1980, *Appl. Opt.*, **19**, 1519-1522.
- Shao, M.; Colavita, M. M.; Hines, B. E.; Staelin, D. H.; Hutter, D. J., 1988, *A&A*, **193**, 357.
- Shao, M., Colavita, M. M., 1992b, *A&A*, 262, 353
- Thompson, A.R., Moran, J.M., Swenson, G.W., 2001, *Interferometry and synthesis in radio astronomy*, 2nd Ed., New York : Wiley
- Traub, W., Carelton, N., Porro, I. *JGR*, 101, Issue E4, April 25, 1996, pp.9291-9296
- Vogt, S. S., Marcy, G. W., Butler, R. P., & Apps, K. 2000, *ApJ*, **536**, 902
- Whitmire, D. P., Matese, J. J., Criswell, L., & Mikkola, S. 1998, *Icarus*, **132**, 196
- Woitaz, J., Tamazian, V. S., Docobo, J. A., Leinert, Ch., 2003, *A&A*, **406**, 293-298.
- Worley, C.E., Mason, B.D., & Wycoff, G.L. 2001, *USNO Photometric Magnitude Difference Catalog*, <http://ad.usno.navy.mil/wds/dmtext.html>